Published in final edited form as:
Nano Lett. 2009 July ; 9(7): 2736–2741. doi:10.1021/nl901534q.

Long Term Persistence and Spectral Blue Shifting of Quantum Dots in vivo

James A.J. Fitzpatrick†, **Susan K. Andreko**, **Lauren A. Ernst**, **Alan S. Waggoner**[a], **Byron Ballou**, and **Marcel P. Bruchez**[b]
Molecular Biosensor and Imaging Center, Carnegie Mellon University, 4400 Fifth Avenue, Pittsburgh PA 15213 bruchez@andrew.cmu.edu

Abstract

Quantum dots are a powerful fluorophore family with desirable attributes for fluorescence imaging. They have been used in several animal models with direct clinical relevance, including sentinel lymph node mapping, tracing vasculature and lymphatics, and targeting specific lesions for diagnosis and removal [1–12]. Despite significant interest for use in translational applications, little is known about the persistence and long-term fate of quantum dots in vivo. We have observed fluorescence of quantum dots injected into Balb/c and nude mice for up to two-years post injection using both whole-body and microscopic fluorescence techniques. Two-photon spectral microscopy was used to verify the existence of quantum dots within two-year tissues, but also revealed a range of significantly blue shifted emission peaks with increased bandwidths. Systemically administered quantum dots persist and retain fluorescence for up to two-years in vivo, but with significantly blue-shifted emission.

Keywords

Quantum dots; in vivo; imaging; whole animal fluorescence; microscopy; two-photon; spectral analyses

---

Quantum dots were supplied by Quantum Dot Corporation, now a division of Invitrogen Corporation (Eugene, OR). For the experiments reported here, 655nm emitting ZnS capped CdSe quantum dots were used exclusively. The coating was the standard primary amphiphilic polymer coat[13], with mPEG-5000 conjugated to the outer coating, analogous to the Q-Tracker non-targeted quantum dots available from Invitrogen (Eugene, OR). These quantum dots are rod-shaped with an aspect ratio of ~2.2:1 which has previously been confirmed by Transmission Electron Microscopy (TEM) [14].

All animal experiments were approved by the IACUC at Carnegie Mellon University. Mice (BALB/c and nude) were obtained from Harlan Sprague Dawley (Indianapolis, IN). Nude mice were used to minimize any background due to intrinsic fluorescence from fur. Quantum dots (typically 480 picomoles, ~170 μg cadmium ion; equivalent to 8.5mg/kg as Cd^{++}, about 2 lethal doses of Cd^{++} as $CdCl_2$ i.v.[15]) were injected by tail vein. Whole-animal imaging was as described;[3] briefly, images were acquired using a either a Photometrics C258 deep-cooled

†fitzp@andrew.cmu.edu.
[a]Department of Biological Sciences, Carnegie Mellon University
[b]Department of Chemistry, Carnegie Mellon University

SUPPORTING INFORMATION PARAGRAPH Supplementary information contains 1. Blinded and 2. non-blinded veterinary pathologist reports, 3. mouse designations, 4. autofluorescence whole animal images and 5. TEM images (low and high magnification) of nanocrystals in lymphatic tissues obtained from one of the two-year old mice.

CCD (Photometrics Tucson, AZ 85706) equipped with a custom filter holder and lens adapter (Bioptics, Butler, PA) or an Andor DU 434-BRDD cooled CCD camera (Andor Technology, South Windsor, CT). Animals were typically illuminated by four 250-watt quartz-halogen illuminators (Cuda Products, Jacksonville, FL) equipped with half-inch fiber optic bundles terminating in filter holders (Edmund Industrial Optics, Barrington, NJ). Excitation filters were 460/50nm and the emission filter was a 654×24nm band pass filter, all provided by Chroma Technologies (Brattleboro, VT). Imaging times varied with time post-injection, and were adjusted on the fly to give maximum dynamic range, but were typically 0.5s; acquisition times of 0.2, 1.0, and 5s were sometimes used to bracket the large range in intensities between different sites of deposition or to reveal faint fluorescence.

All spectral measurements were undertaken using an inverted Axio Observer Z1 motorized microscope with an LSM 510 Meta NLO confocal scan head (Carl Zeiss, Jena, Germany) coupled to a Chameleon Ultra-II femtosecond titanium sapphire laser (Coherent Laser Inc., Santa Clara, CA) as the two-photon excitation source. Once a particular area within a given tissue sample had been identified by both brightfield (targeting of specific cellular structures, e.g., germinal centers) and epi-fluorescence (to confirm presence of quantum dots), two-photon confocal microscopy was performed using a 10X Plan-NeoFluar (0.3NA 5.5mm WD) dry objective lens with the frozen section mounted on a type 1 coverslip.

Spectral data were acquired using 890nm excitation light from the titanium sapphire laser and was directed to the sample using a 725nm short pass dichroic mirror. Confocal fluorescence was extracted through that mirror, passed through BG39 glass to block any stray two-photon excitation light and sent to the Meta spectral detector (collected range 500–700nm). Spectral images were acquired as averages of four independent scans. A maximum projection image of all spectral slices was plotted and individual regions of interest were designated (i.e. autofluorescent structures, or clusters of quantum dots). The intensity of each of those areas was integrated in each spectral slice, and then normalized and plotted as a function of wavelength. Peak positions and widths were obtained for each designated region of interest by taking the emission profile and fitting it to a single-component Gaussian function with both peak position and width parameters. For emission profiles that clearly had a secondary blue-shoulder, a second Gaussian function was added to the model to enable fitting. Each fit routinely yielded $R^2 > 0.96$ for the single component model and $R^2 > 0.89$ for the two-component model. Spectra of nominally quantum dot regions were identical under both 890 and 960nm two-photon excitation.

This procedure was undertaken over multiple tissue samples and types to ensure a fair representation of the complete dataset. In order to ensure that the Meta detector was sufficiently calibrated before these studies were commenced, spectra were obtained from solutions of organic dyes (Cy2, Cy3 and Cy5) and a range of quantum dot samples (585, 605, 655 and 705nm ITK-carboxyl dots). Spectra obtained from the Meta detector were compared with spectra obtained from the same samples on a Tecan Safire2 fluorescence plate reader. No obvious discrepancy between the two sets of spectral curves was observed.

A total of 23 mice were imaged at intervals from 15min to two years after tail-vein injection of quantum dots; only the five mice (3 Balb/c, 2 nude, all female) who survived for two years are described here. Three additional historical controls, Balb/c aged 1 year and 6 months, were also examined. After imaging, mice were necropsied; tissues were removed including liver, spleen, bone marrow and lymph nodes for examination and were divided into two portions. (1) Samples were frozen immediately in Tissue-Tek OCT embedding compound (Sakura Finetek, Torrance, CA) and used to prepare frozen sections all of which were examined by two-photon spectral microscopy. (2) Tissue samples for standard pathological examination were placed directly into 5% formaldehyde until sent to two separate veterinary pathologists,

one of whom was double blinded and one who was not; both were requested to examine the tissues, with particular regard to any abnormalities in the reproductive organs (both pathology reports are available in the Supplementary Data). The tissues were subjected to paraffin embedding, sectioning, and hematoxylin-eosin staining in the pathological laboratory using standard methods. Tissue sections were imaged by brightfield and fluorescence microscopy to identify tissue types and to target locations in which to make two-photon confocal measurements of the fluorescence spectra originating from specific cellular structures.

Immediately after injection, quantum dot fluorescence was seen in the circulation, liver, spleen, lymph nodes, and bone marrow. Quantum dots are rapidly cleared from the circulation into the RES, with a lifetime that is dependent on the nanocrystal coating[3, 4, 6, 12]. With increasing time post-injection, the liver fluorescence rapidly faded (2–5 days); the fluorescence in the bone marrow faded more slowly (3–6 months), while the lymph nodes retained quantum dot fluorescence for a longer period (upto 2 years). It is unclear at this time whether this fading of fluorescence is due to particle dissolution, darkening or excretion mechanisms. While there was considerable inter-mouse variability in the absolute amounts of material retained as assessed by fluorescence, this pattern of successive fluorescence loss from different organs was invariant among mice, and was similar in pattern and timing whether Balb/c or nude mice were used.

Figure 1 shows a nude mouse, necropsied two years post-injection. By this time, grossly visible quantum dot fluorescence had disappeared from all organs except the lymph nodes, which retained low-level fluorescence. Because the fluorescence originating from the lymph nodes was weak, two-photon spectral confocal microscopy was required to verify the continued presence of quantum dots (whose red emission spectra are significantly different from that of the predominantly green/yellow autofluorescence). We found that quantum dots could still be detected by fluorescence microscopy in the liver and the spleen as well as the lymph nodes, even though they were not easily visualized by gross fluorescence imaging[1]. Essentially all quantum dots were in clusters containing multiple quantum dots (presumably in vesicles[3]); no individual quantum dots were seen as evidenced by the lack of fluorescence blinking events and the very high signal over tissue autofluorescence (Figure 2e).

Fluorescence images taken from a spectral stack of a frozen section of a two-year lymph node are shown in Figure 2. Panel **a** shows a projection of 5 spectral slices ranging from 500–550nm and is pseudo-colored green. This spectral region predominantly shows tissue background autofluorescence. Panel **b** shows a DIC image taken of the same tissue region to show the morphology of the lymph node. Panel **c** shows a second projection of 5 spectral slices, this time ranging from 620–670nm pseudo-colored red. This spectral region encompasses the majority of the quantum dot emission. Finally, panel **d** shows an overlay of the green and red spectral regions illustrating the lack of co-localization of the fluorescence signals, demonstrating that the quantum dot fluorescence is distinct from the tissue background (note that the background autofluorescence is almost a factor of 10 weaker than the quantum dot fluorescence, even after 2 years. For clarity, the lookup-table in panel **a** has been adjusted to display at a brightness level similar to that of panel **c**). To further confirm the identity of the quantum dots visualized in the two-year lymph node, spectra obtained from red fluorescent objects were plotted and fitted to Gaussian function(s) to provide peak position and spectral width. Surprisingly, fluorescence originating from clusters of quantum dots, although characteristically sharp peaked, appeared to be significantly blue-shifted (Figure 2e) from the expected peak position of 655nm. This is in contrast to the previously reported red-shifting behavior of clusters of quantum dots[16]. Systematic examination and fitting of multiple clusters of quantum dots dispersed throughout the lymph node tissue revealed a range of peak positions blue-shifted up to 40nm (Figure 2e), some even having a multi-peak emission profile with a sub-population shifted to the blue by almost 70nm (Figure 2e).

The background fluorescence from non-quantum dot areas (Figure 2e, **green circles**), and from un-injected animals (Figure 2e, **open green circles with dashed line**), was easily distinguished from the quantum dot emission by spectral profiles. Both background and quantum dot emission profiles are inconsistent with lipofuscin autofluorescence, reported to peak near 580 nm[17]. As an additional spectral control, the two-photon excitation wavelength was shifted to the red in an effort to minimize excitation of autofluorescence. Since quantum dots have an unusually flat two-photon excitation cross-section[18], it is expected that the tissue background will be significantly reduced and the quantum dot signal will remain the same. At a two-photon excitation wavelength of 960nm, the tissue background had almost completely disappeared whereas the quantum dot signal was as strong as when excited at 890nm, with no shift in the observed quantum dot emission spectra. In addition, freshly injected control animals, whose organs were harvested 24h post-injection showed that the 655nm quantum dots retained their fluorescence, and were easily distinguished against the tissue background (which was almost nonexistent in the younger animals). The spectral emission of the quantum dots was characteristically sharp-peaked with a maximum at 655nm, as expected (Figure 2e, **open black squares**). This reconciles almost perfectly with the peak position and width obtained from the fluorescence spectrum of 655nm emitting quantum dots in solution (Figure 2e, **black dotted line**).

Examination of spectral datasets obtained from frozen sections of the liver, spleen and lymph nodes from the same two-year mouse showed a similar range of blue-shifted peak positions in the quantum dot emission profiles. Liver, spleen and lymph node tissues from the four remaining two-year mice (two nude and two Balb/C) were subjected to the same spectral analyses. Confirming our previous observation, a range of blue-shifted quantum dot emission peaks was observed in the all examined tissues in each of the remaining two-year mice. Figure 3a illustrates the same data plotted as a histogram. Data from the 24h control mouse tissues shows the fitted peak positions clustered around 655nm with data from the two-year tissues primarily clustered around in the range 620–650nm with a smaller number of occurrences in the range 570–610nm. Bars denoted with an asterisk identify a peak position that was a blue shoulder in a fitted secondary sub-peak in the emission profile. It is interesting to correlate the variation in the fitted 1/e spectral width (s) of the quantum dot emission profiles with the blue-shifted peak position (Figure 3b). The 24h control tissues are clustered around 655nm with a width range of 12–18nm. The two year tissues cluster in the range 620–650nm with a width range of 15–30nm. Peak positions that originate from a sub-peak in an emission profile cluster in the range 580–610nm (as identified with an asterisk), and have a substantially increased width (range 35–80nm). P-values for the fitted peak positions were calculated between each two-year tissue type and between a given two-year and 24h tissue type with Welch's T-Test using a two tail distribution and a either an equal (for two-year tissues) or unequal variance (two year and 24h tissues). Each of two-year tissue correlations exhibited a significant p-value, Lymph nodes : Liver = 0.6, Lymph nodes : Spleen = 0.71 and Liver : Spleen = 0.36, indicating that each distribution had a similar mean peak position value. The contrasting results from analysis of the same two-year and 24h tissues shows no statistically significant similarities between the mean value of the peak positions, 2yr Lymph nodes : 24h Lymph nodes = 8.9e-7, 2yr Liver : 24h Liver = 1.7e-6 and 2yr Spleen : 24h Spleen = 3.1e-7

It is significant that the abnormal quantum dot emission profiles were not seen in any mice whose organs were harvested soon after injection, even when the freshly harvested tissues had also been kept frozen at −80°C for as long as two years. Thus the blue shift in peak positions cannot be attributed to storage and was due solely to the long residence time in living animals. The simplest interpretation of the blue shift seen in quantum dot fluorescence after two years in vivo is a slow breakdown of the quantum dots; a degradation of the ZnS surface and/or slow loss of core, a cationic exchange mechanism or a change in a the size-shape aspect ratio of the nanocrystal could yield the range of blue shifts seen here[19, 20]. It is important to note that the

range of observed blue shifts is tissue type invariant eliminating organ-specific breakdown mechanisms. This suggests that the degradation mechanism may be specific to subcellular location (ie vesicle physiology; presence of peroxide, pH level) or simply a result of long-term infinite dilution. Such mechanisms function by exchange of inorganic components with ions in the environment and would result in a potential release of heavy metals. These quantum dots caused no acute toxicity when injected in quantities that would normally be expected to show lethal toxicity as soluble cadmium ions; and, at least some of the particles remain fluorescent for as long as two years. The quantum dot core and shell must have remained relatively intact to have retained detectable fluorescence over such a long period, and leakage of cadmium ions is likely at a low level. However, the appearance of a wavelength shift strongly argues that the particles, in spite of both a ZnS and polymer coat, are degraded over time in vivo. Low-level toxicity would not have been evident in these experiments due to the small number of animals and organ degeneration with age; especially in the pathological analysis, given the typical shrinkage and impoverishment in the cellular content of lymph nodes in both normal and nude aged animals.

There have been many tests of quantum dot toxicity on tissue-cultured cells, based on either concentration or uptake[19] (for review, see Cai et al[5]. and Lewinski et al.[11]). The results have been mixed. Core-only quantum dots have proved toxic, both by release of heavy metals and possibly through other effects[21–26]. Core-shell quantum dots are far less toxic, and toxicity from surface-protected core-shell quantum dots (silica or polymer coated) has been minimal (*ibid*., and see references[27–29]). Some surface coatings can predispose to toxicity, and some may be toxic themselves[23, 30]. Effects on gene expression and differentiation by surface-coated quantum dots have been noted; it is not clear whether these effects are significant[29, 31–33].

Quantitative biodistribution studies in whole animals have used radioactively labeled quantum dots[4, 6, 12, 21]. All studies find short-term retention of quantum dots in tissues (on the order of days to 1 week); especially RES tissues, though the specific organ distribution varies with the surface coat. Contrary to our findings[3], other workers[6] found essentially no fecal excretion of quantum dots; probably due to the different surfaces they used. On the other hand, Choi et al. [21] found rapid clearance through the kidneys when using sufficiently small quantum dots coated by cysteine. Their work offers a novel path to the future; less toxic formulations of quantum dots, and designs for rapid clearance should minimize toxicity in vivo. Our results also indicate that biodistribution analyses should consider both the presence of ionic and particle species for a rugged analysis.

The emerging picture of Cd based quantum dot toxicity suggests that quantum dots require improvements before they can be safely used in clinical settings, but offers hope that improved materials could become useful optical probes. The short-term stability, but the potential for long-term breakdown of nanoparticles in vivo simultaneously reduces the fears of acute metal toxicity, and increases the concerns of chronic toxicity, especially because of the long metabolic lifetime of cadmium in humans[34]. Our results indicate that even very robust particle coatings do not prevent subsequent breakdown in vivo. It is therefore necessary to develop particle chemistries that avoid the use of toxic metals and that ensure rapid clearance of quantum dots and their breakdown products before they can be used in any but the most dire clinical applications.

Supplementary Material

Refer to Web version on PubMed Central for supplementary material.

Acknowledgments

The authors wish to acknowledge the NIH BRP program under grant number 5R01EB00364 and the NIH Technology Center for Networks and Pathways under grant number 5U54RR022241 for financial support and to Dr Justin Crowley in the Department of Biological Sciences at Carnegie Mellon University, for facilitating the use of his two-photon spectral confocal microscope for the initial experiments in this study. MB also wishes to acknowledge Carnegie Mellon University for faculty start-up funds.

References

1. Akerman ME, Chan WC, Laakkonen P, Bhatia SN, Ruoslahti E. Proc Natl Acad Sci U S A 2002;99 (20):12617–21. [PubMed: 12235356]
2. Ballou B, Ernst LA, Andreko S, Harper T, Fitzpatrick JAJ, Waggoner AS, Bruchez MP. Bioconjugate Chemistry 2007;18(2):389–396. [PubMed: 17263568]
3. Ballou B, Lagerholm BC, Ernst LA, Bruchez MP, Waggoner AS. Bioconjug Chem 2004;15(1):79–86. [PubMed: 14733586]
4. Cai W, Chen K, Li ZB, Gambhir SS, Chen X. Journal of Nuclear Medicine 2007;48(11):1862–1870. [PubMed: 17942800]
5. Cai W, Hsu AR, Li ZB, Chen X. Nanoscale Research Letters 2007;2(6):265–281.
6. Fischer HC, Liu LC, Pang KS, Chan WCW. Adv Funct Mater 2006;16(10):1299–1305.
7. Frangioni, JV.; Kim, SW.; Ohnishi, S.; Kim, S.; Bawendi, MG. Methods in molecular biology. Clifton, NJ., editor. Vol. 374. 2007. p. 147-59.
8. Gao X, Cui Y, Levenson RM, Chung LW, Nie S. Nat Biotechnol 2004;22(8):969–76. [PubMed: 15258594]
9. Gopee Neera V, Roberts Dean W, Webb P, Cozart Christy R, Siitonen Paul H, Warbritton Alan R, Yu William W, Colvin Vicki L, Walker Nigel J, Howard Paul C. Toxicol Sci 2007;98(1):249–57. [PubMed: 17404394]
10. Hama Y, Koyama Y, Urano Y, Choyke PL, Kobayashi H. Breast cancer research and treatment 2007;103(1):23–8. [PubMed: 17028977]
11. Lewinski N, Colvin V, Drezek R. Small (Weinheim an der Bergstrasse, Germany) 2008;4(1):26–49.
12. Schipper ML, Cheng Z, Lee SW, Bentolila LA, Iyer G, Rao J, Chen X, Wu AM, Weiss S, Gambhir SS. J Nuc Med 2007;48(9):1511–1518.
13. Wu X, Liu H, Liu J, Haley KN, Treadway JA, Larson JP, Ge N, Peale F, Bruchez MP. Nat Biotechnol 2003;21(1):41–6. [PubMed: 12459735]
14. Giepmans BNG, Deerinck TJ, Smarr BL, Jones YZ, Ellisman MH. Nat Meth 2005;2(10):743–749.
15. Cantilena LR Jr, Klaassen CD. Toxicol Appl Pharmacol 1980;53(3):510–4. [PubMed: 6770496]
16. Leatherdale CA, Kagan CR, Morgan NY, Empedocles SA, Kastner MA, Bawendi MG. Phys Rev B 2000;62(4):2669.
17. Stark WS, Miller GV, Itoku KA. Methods in enzymology 1984;105:341–7. [PubMed: 6727675]
18. Larson DR, Zipfel WR, Williams RM, Clark SW, Bruchez MP, Wise FW, Webb WW. Science 2003;300(5624):1434–6. [PubMed: 12775841]
19. Chang E, Thekkek N, Yu WW, Colvin VL, Drezek R. Small (Weinheim an der Bergstrasse, Germany) 2006;2(12):1412–7.
20. Dabbousi BO, Rodriguez-Viejo J, Mikulec FV, Heine JR, Mattoussi H, Ober R, Jensen KF, Bawendi MG. J Phys Chem B 1997;101(46):9463–9475.
21. Choi HS, Liu W, Misra P, Tanaka E, Zimmer JP, Ipe BI, Bawendi MG, Frangioni JV. Nat Biotechnol 2007;25(10):1165–1170. [PubMed: 17891134]
22. Derfus AM, Chan WCW, Bhatia SN. Nano Lett 2004;4(1):11–18.
23. Hoshino A, Fujioka K, Oku T, Suga M, Sasaki YF, Ohta T, Yasuhara M, Suzuki K, Yamamoto K. Nano Lett 2004;4(11):2163–2169.
24. Kirchner C, Liedl T, Kudera S, Pellegrino T, Munoz Javier A, Gaub HE, Stolzle S, Fertig N, Parak WJ. Nano Lett 2005;5(2):331–8. [PubMed: 15794621]

25. Lovric J, Cho SJ, Winnik FM, Maysinger D. Chemistry & biology 2005;12(11):1227–34. [PubMed: 16298302]

26. Shiohara A, Hoshino A, Hanaki K, Suzuki K, Yamamoto K. Microbiology and immunology 2004;48 (9):669–75. [PubMed: 15383704]

27. Chen F, Gerion D. Nano Letters 2004;4(10):1827–1832.

28. Tan TT, Selvan ST, Zhao L, Gao S, Ying JY. Chemistry of Materials 2007;19(13):3112–3117.

29. Zhang TT, Stilwell JL, Gerion D, Ding LH, Elboudwarej O, Cooke PA, Gray JW, Alivisatos AP, Chen FF. Nano Lett 2006;6(4):800–808. [PubMed: 16608287]

30. Ryman-Rasmussen JP, Riviere JE, Monteiro-Riviere NA. Journal of Investigative Dermatology 2007;127(1):143–153. [PubMed: 16902417]

31. Chakraborty SK, Fitzpatrick JA, Phillippi JA, Andreko S, Waggoner AS, Bruchez MP, Ballou B. Nano Lett 2007;7(9):2618–26. [PubMed: 17663586]

32. Hsieh SC, Wang FF, Hung SC, Chen YJ, Wang YJ. J Biomed Mater Res B Appl Biomater 2006;79B (1):95–101. [PubMed: 16470833]

33. Hsieh SC, Wang FF, Lin CS, Chen YJ, Hung SC, Wang YJ. Biomaterials 2006;27(8):1656–1664. [PubMed: 16188313]

34. Sugita M, Tsuchiya K. Env Res 1995;68(1):31–7. [PubMed: 7729385]

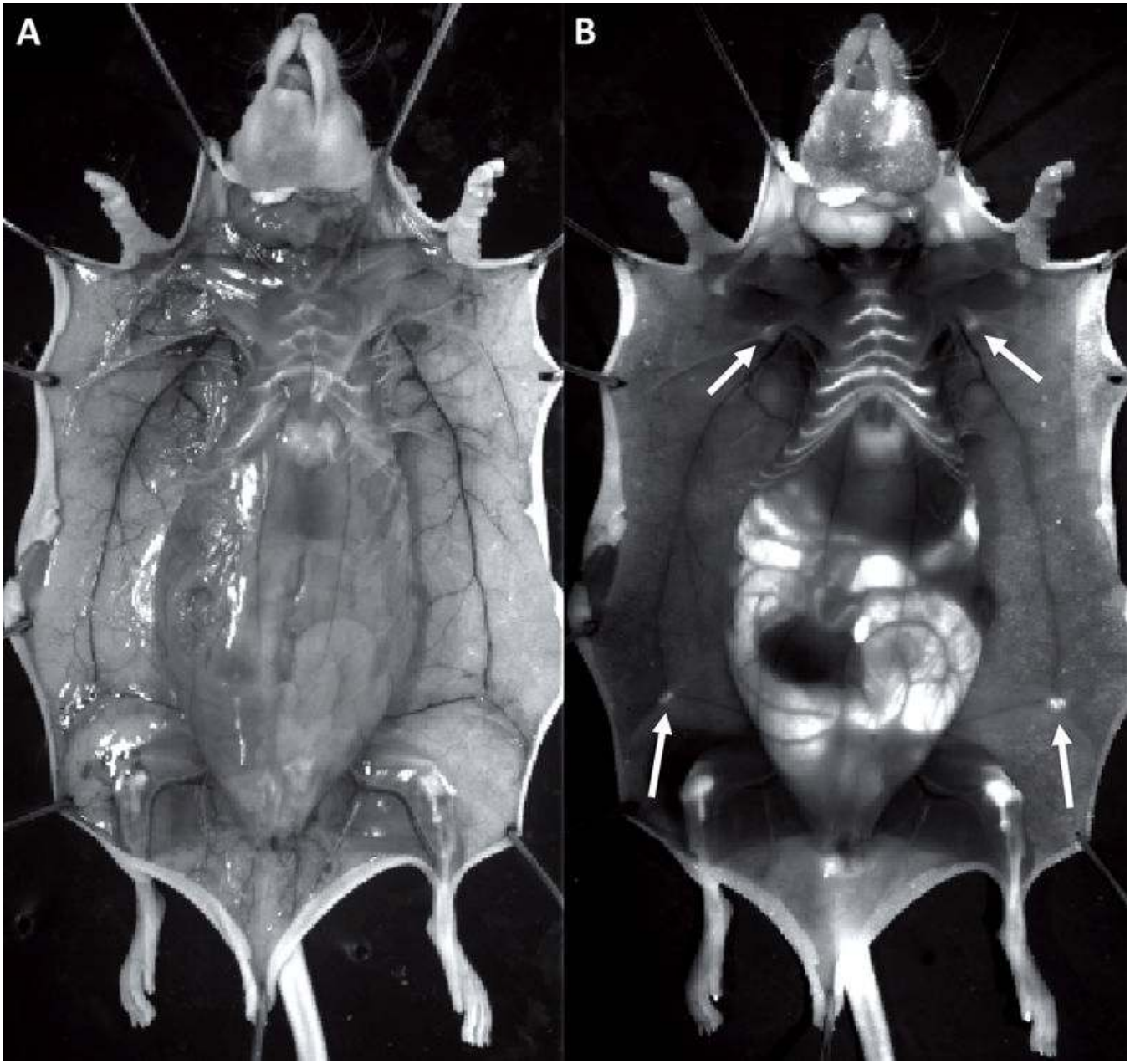

Figure 1. Nude mouse visualized 2 years post-injection

a visible light; **b.** 655nm fluorescence. Despite high intrinsic fluorescence from the intestines, sufficient quantum dot signal exists to distinguish the inguinal and axiliary lymph nodes (indicated by white arrows). The bright spots evident in the hind legs result from autofluorescent cartilage in the kneecaps. This is mouse 7 in the Supplementary Data Table.

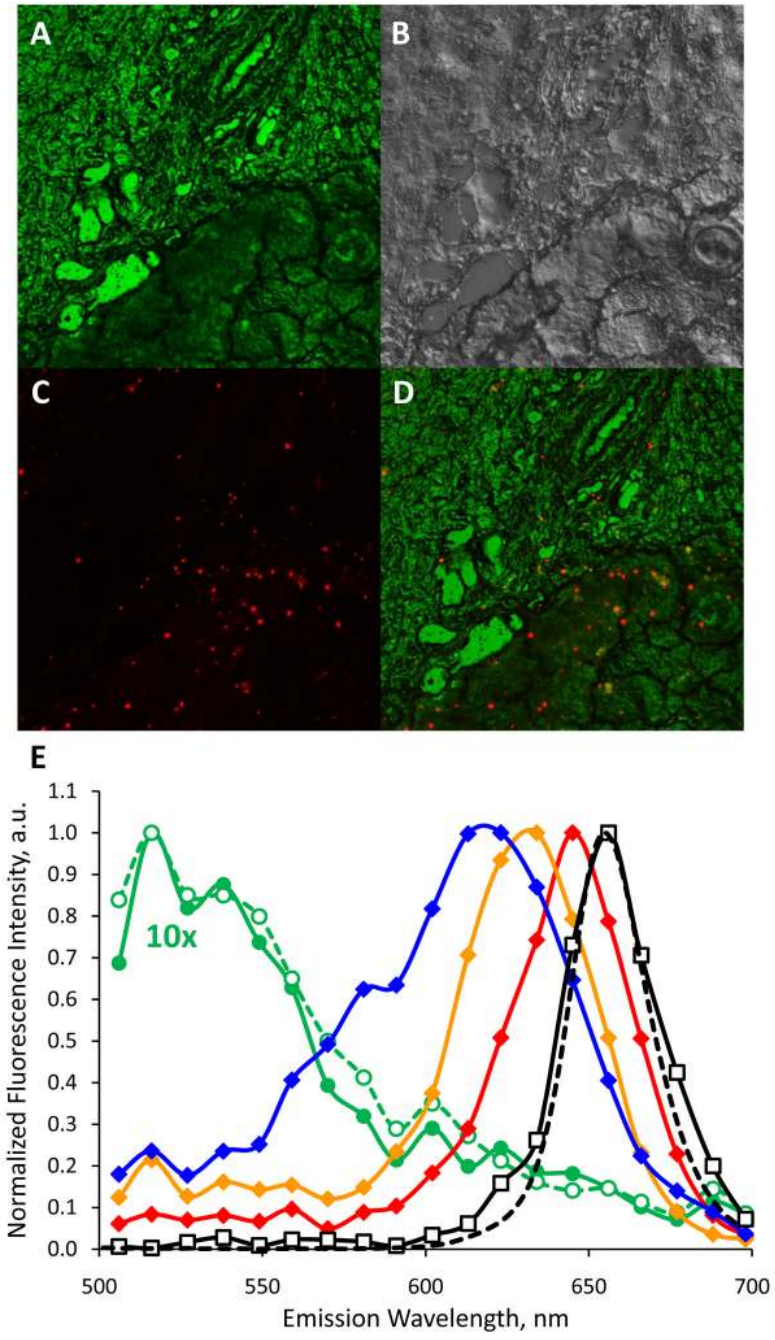

Figure 2. Confocal fluorescence images and normalized spectral emission data from frozen lymph node sections from control (24h) and 2yr mice

a projection of 5 spectral slices ranging from 500–550nm from a frozen section of a 2yr lymph node pseudo-colored green. This spectral region predominantly shows tissue background autofluorescence. **b.,** transmitted light DIC image taken of the same tissue region in **a,** to illustrate the morphology of the lymph node. **c.,** projection of 5 spectral slices ranging from 620–670nm from the same frozen section pseudo-colored red. This spectral region encompasses the majority of the quantum dot emission. **d.,** overlay of the green and red spectral regions illustrating the lack of co-localization of the fluorescence signals, **e.,** Normalized spectral data from frozen tissue sections. 24h injected control mouse lymph node (black open

squares); 2yr mouse lymph node region 1 (red diamonds); 2yr mouse lymph node region 2 (orange diamonds); 2yr mouse lymph node region 3 (blue diamonds); 2yr mouse autofluorescence (green circles) and 18mo un-injected control mouse autofluorescence (open green circles with dashed line, whole animal white light and fluorescence image shown in Supplementary Data). The black dotted line represents the fluorescence spectrum from 655nm emitting quantum dots taken in solution. Note the almost identical peak position and width as those taken from the 24hr injected mouse (black open squares). Note the unaltered spectral emission of the quantum dots in tissue harvested soon after injection compared to the large range of changes observed in those tissues harvested 2 years after injection. The autofluorescence intensity was a factor of ten less than that of the quantum dots and both the autofluorescence from the 2yr injected mouse and the 1.5 year un-injected mouse have similar spectral signatures. The 2yr mouse is mouse 3 (BALB/c); the 1.5yr mouse is mouse 2 (also BALB/c) in the Supplementary Data Table.

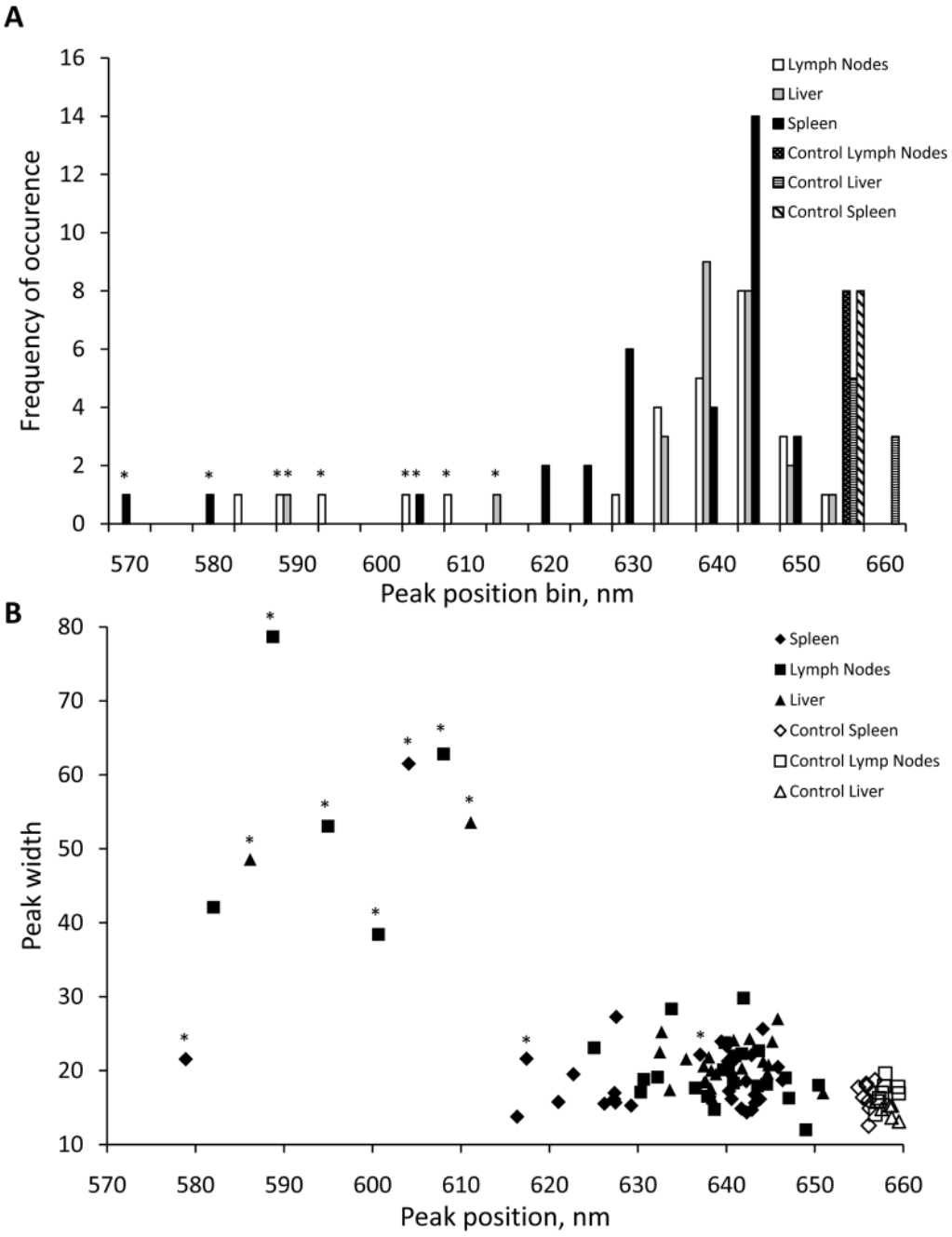

Figure 3. Fitted quantum emission profile peak positions and spectral widths from lymph node, liver and spleen tissues from control and 2yr mice

a Histogram of fitted peak positions of lymph node, liver and spleen tissues from control (n=3) and 2yr (n=5) mice, **b.,** Plot of fitted peak positions against spectral widths. Note that bars denoted with an asterisk identify peak positions that were fitted as a sub-peak originating from a blue shoulder in a quantum dot emission profile. Plotted widths are actually the fitted 1/e width (s) and not the full-width half-maximum.